The Astrophysical Journal Supplement Series, 224:17 (7pp), 2016 June doi:10.3847/0067-0049/224/2/17

INFRARED AND ULTRAVIOLET SPECTRA OF METHANE DILUTED IN SOLID NITROGEN AND IRRADIATED WITH ELECTRONS DURING DEPOSITION AT VARIOUS TEMPERATURES

Chih-Hao Chin[1], Sian-Cong Chen[1], Meng-Chen Liu[1], Tzu-Ping Huang[1], and Yu-Jong Wu[1,2]
[1] National Synchrotron Radiation Research Center, No. 101, Hsin-Ann Road, Hsinchu Science Park, Hsinchu 30076, Taiwan; yjwu@nsrrc.org.tw
[2] Department of Applied Chemistry and Institute of Molecular Science, National Chiao Tung University, 1001, Ta-Hsueh Road, Hsinchu 30010, Taiwan
Received 2016 January 25; accepted 2016 March 23; published 2016 May 26

ABSTRACT

We recorded the infrared and ultraviolet absorption spectra of CH_4:N_2 matrix samples that underwent electron bombardment during deposition in the temperature range of 10–44 K. In contrast to a previous experiment on the IR spectroscopy of electron-bombarded icy samples, methyl and azide radicals became the main products upon electron bombardment during deposition; furthermore, reduced production of nitrile species was observed for deposition at 10 and 20 K. On the other hand, for deposition above 33 K, the observed bands of the radical species (such as methyl and azide) decreased, and bands of large nitriles appeared. This observation may suggest that radical species easily diffuse and recombine to form more complex molecules in solid nitrogen at higher temperatures. Further measurements of similar samples at 10–33 K in the UV region revealed the intense band of azide radicals at 272.5 nm and weak, broad, overlapping features of methyl and azide radicals in the 225–197 nm region. For deposition at 44 K, only a broad feature centered at 219.4 nm was observed, and the possible carriers of nitrile species were proposed based on the corresponding IR spectrum and theoretical predictions of excitation energy. This band is similar to the observed absorption feature of Pluto's surface recorded by the *Hubble* telescope in terms of both band position and bandwidth. Our findings therefore further support the suggestion that complex nitrile species may exist on the surface of Pluto.

Key words: astrochemistry – Kuiper Belt objects: individual (Pluto) – methods: laboratory: molecular – molecular processes

1. INTRODUCTION

Pluto, the largest dwarf planet (by volume) found in the Kuiper Belt, was discovered in 1930, and in the following decades was spectroscopically probed in the ultraviolet (UV) to infrared (IR) region using telescopes (Cruikshank et al. 1976; Owen et al. 1993; Krasnopolsky 2001; Stern 2010; Tegler et al. 2010; Lellouch et al. 2011; Grundy et al. 2013). A tenuous atmosphere that consists of nitrogen, methane, and carbon monooxide—with an atmospheric pressure of about 10 μbar near the surface—has been confirmed on Pluto (Stern et al. 2015). Furthermore, the surface is covered by ices with similar compositions (Stern 2010; Tegler et al. 2010; Grundy et al. 2013). Pluto's orbit is elliptic, and its distance from the Sun ranges from 49 to 30 au, which results in a variable surface temperature of 33–55 K. Some volatile surface ices, such as N_2, CO, and CH_4, thus sublimate to the atmosphere. In addition to the compositional variation between the atmosphere and surface on a seasonal timescale, the compositions of CO and N_2 ices are also found to be strongly associated with Pluto's 6.4 day rotation (Cruikshank et al. 2015; Merlin 2015). This dynamical equilibrium between atmosphere and surface is expected to be one of the main reasons for the high surface reflectivity of ~60% (Schindhelm et al. 2015).

The *New Horizons* spacecraft was launched in 2006 in order to study the Pluto system and other Kuiper Belt objects, and encountered Pluto on 2015 July 14 (Stern et al. 2015). During its brief flyby, detailed measurements and new discoveries of Pluto and its moons were made. More specifically, it was discovered that Pluto's atmosphere extends to a height of 1670 km above the ground; furthermore, the existence of C_2H_2 and C_2H_4 was confirmed for the first time at altitudes below 420 km, with mixing ratios of about 10^{-6}. The fractional number density abundance of atmospheric CH_4 was also determined to be ~0.25%, which is slightly lower than previous estimates (Owen et al. 1993; Lellouch et al. 2011). In addition, a global haze layer was observed at altitudes below 150 km (Stern et al. 2015; Gladstone et al. 2016). In terms of surface ices, N_2, CH_4, and CO ices were observed to dominate and to be widely distributed, although this might only represent a surface veneer above the water-ice-based solid. The observed natural colors on Pluto's surface, ranging from yellow to dark red, suggest that refractory organic residuals (tholins) are formed through the complex radiation chemistry occurring in both atmosphere and surface ices. Solar ultraviolet light, cosmic rays, and solar wind can dissociate CH_4 in the upper atmosphere, which leads to the formation of other atmospheric components, such as C_2H_2 and C_2H_4. These larger hydrocarbons condense as ice particles to form hazes in the lower atmosphere. These hazes then further react with surrounding N_2 and become chemically converted into more complex molecules (tholins), which fall into Pluto's surface (Cruikshank et al. 2005, 2015; Stern et al. 2015; Grundy et al. 2016). The mechanism mentioned above is supported by astronomical observations of hazes and images of icy surfaces; however, the detailed pathways from predominant atmospheric and icy components in the molecular level are not well understood.

The irradiation of ice mixtures that are known to be components on Pluto with ultraviolet light and energetic particles in laboratories has been extensively studied over the past two decades. The results of laboratory simulations of binary N_2–CH_4 ices and ternary N_2–CH_4–CO ices irradiated with 0.8 MeV protons (Hudson & Moore 2002), ultraviolet light (Milligan & Jacox 1967; Bohn et al. 1994; Hudson & Moore 2002; Hodyss et al. 2011; Wu et al. 2012; Materese et al. 2014; Lo et al. 2015), electrons (Kim & Kaiser 2012; Wu et al. 2013a; Materese et al. 2015), and heavy ions (Palumbo

et al. 2004) suggest that these forming products, which include hydrocarbons and nitriles in neutral and ionic forms, might exist on Pluto's surface. However, none of the proposed molecules has been clearly identified. In these previous works, the irradiation of mixtures was performed in the ice phase. In this work, the irradiation of CH_4/N_2 gaseous mixtures with electrons was carried out, and then followed by condensation onto the cold target to form ice samples at various temperatures. We used electrons with energies of 500 eV this was done because a few hundred electronvolts corresponds to the resonant energy for the ionization or dissociation of molecules caused by the electronic excitation of core-level electrons of molecules (Eberhardt et al. 1983a, 1983b; Mangina et al. 2011; Song et al. 2015). Methane and nitrogen both show considerable electron-impact cross sections and core energy levels around 500 eV; thus, the choice of 500 eV for electron impact can represent typical chemical reactions induced by the electron impact of CH_4:N_2 mixtures.

2. EXPERIMENTAL METHODS

A nickel-plated copper plate serves as a cold substrate for the ice samples. A closed-cycle helium refrigerator system (ARS DE-204) is employed to cool the target. The cryochamber is evacuated by a turbomolecular pump backed with a scroll pump; the base pressure is less than 1×10^{-8} Torr.

A gaseous mixture of CH_4/N_2 at a molar ratio 1/400 was prepared by a manometric (partial pressure) method and stored in a 2-liter steel cylinder in advance. The gas mixture was introduced to the cryochamber from the cylinder directly and was deposited on the cold target over a 4 hr period using a flow rate of 1.0 mmol hr^{-1}. The cold substrate was perpendicular to the direction of the gas beam. We estimated the thickness of the matrix sample at 10 K to be 35–40 μm by measuring the interference fringes of the IR spectrum recorded during the initial period. In separate experiments, the matrix samples were deposited at 20, 33, and 44 K, and the thickness of the matrix samples decreased as the deposition temperature increased. The temperature of the target was monitored and controlled by a temperature controller (Lakeshore 331S) with a calibrated silicon diode (DT-470). The accuracy of temperature measurements fell within $\pm$0.1 K. The gas matrix samples were bombarded during matrix deposition with electron beams generated by an electron gun (energy: 500 eV; beam current: 200 μA; beam diameter: 1 cm; Kimball Physics, Model EFG-7). The electron beam was parallel to the substrate with 2 cm separation, and it interacted with the gas sample within this separation region. The penetration depth of incident electrons into the ice's surface is expected to be less than 50 nm (Barnett et al. 2012; Bennett et al. 2013), and thus only the upper few layers of the matrix sample might be bombarded by scattered electrons. In this manner, the majority of the dissociation/ionization of precursors unambiguously occurs in the gas phase.

IR absorption spectra were recorded using a Fourier transform infrared spectrometer (Bruker, Vertex 80) equipped with a KBr beam splitter and MCT-B detector (cooled to 77 K). The cold target, coated with Ni is polished to serve as a mirror for reflecting the incident IR beam to the detector; the reflection angle of the IR light was 45°. During each stage of the experiments, 400 scans at a resolution of 0.5 cm^{-1} were recorded. UV light was dispersed using a 6 m monochromator on the high-flux beamline of the 1.5 GeV storage ring of NSRRC for measurement of UV absorptions of matrix samples and the spectral resolution was set as 0.2 nm in the wavelength region of 125–350 nm. UV light reflected from the target was detected by a photomultiplier tube (Hamamatsu R6836) with an amplifier (Hamamatsu C7246). CH_4 (99.5%, Matheson Gases) and N_2 gases (99.9995%, Matheson Gases) were used without additional purification.

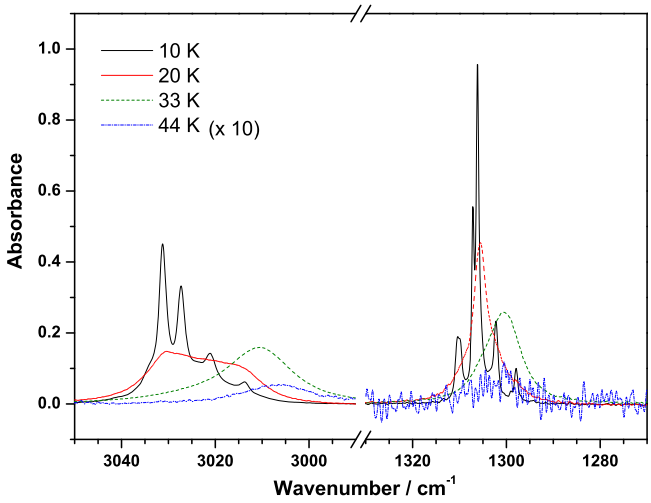

Figure 1. Infrared (IR) absorption spectra of CH_4/N_2 (1:400) matrix samples at various temperatures.

Time-dependent density functional theory (TD-DFT) was employed using the Gaussian 09 program (Frisch et al. 2009) to calculate the vertical excitation energies of low-lying electronic states of $C_3H_2N_2$. The energies and equilibrium structures were calculated using density-functional theory with the B3LYP functional. The B3LYP method uses Becke's three-parameter hybrid exchange functionals and a correlation functional of Lee, Yang, and Parr with both local and nonlocal terms (Lee et al. 1988; Becke 1993). Dunning's correlation-consistent polarized valence triple-zeta basis set, augmented with diffuse functions (aug-cc-pVTZ; Kendall et al. 1992; Peterson et al. 1994), was used in both cases. Analytical first derivatives were utilized in geometry optimization, and vibrational wavenumbers were calculated at each stationary point.

3. RESULTS AND DISCUSSION

3.1. IR Absorption Spectra of CH_4/N_2 Ices

The partial IR absorption spectra of the CH_4/N_2 (1:400) matrix samples deposited at various temperatures are presented in Figure 1. The observed bands are associated with the CH stretching (ν_3) and deformation (ν_4) modes of CH_4 in the spectral regions of 3040–3000 and 1314–1294 cm^{-1}, respectively. The characteristic features of the ν_4 mode at 1310.1, 1306.1 (1307.1), 1302.2, and 1297.8 cm^{-1}—and of the ν_3 mode at 3031.1, 3027.3, 3021.2, and 3013.5 cm^{-1}—were observed for deposition at 10 K. These structures can be attributed to (hindered) rotations and/or multiple trapping sites of CH_4 embedded in a N_2 matrix, which has been discussed in earlier studies (Nelander 1985; Govender & Ford 2000). Upon depositing a CH_4/N_2 sample at 20 K, the ν_4 band became a single symmetric peak at 1305.6 cm^{-1}; the ν_3 band also became a single peak, though it was broad and asymmetric.

The changes of band positions and structures of CH_4 between deposition at 10 and 20 K are due to the different

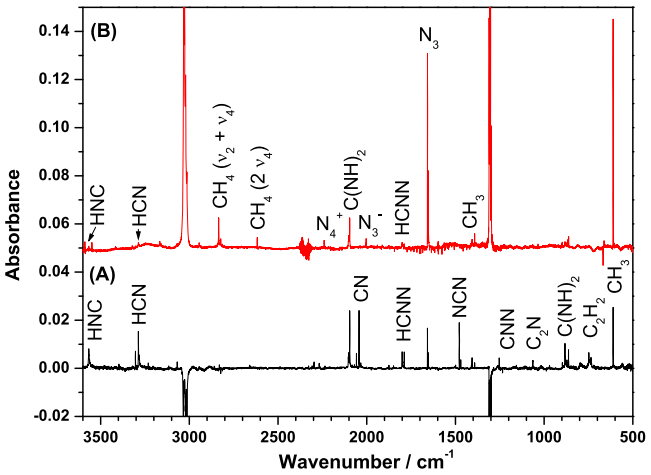

Figure 2. Infrared (IR) spectra recorded after irradiating CH_4/N_2 matrix samples at 10 K (A) after deposition and (B) during deposition with 500 eV electrons. Trace (A), adapted from Wu et al. (2013a), shows a spectrum that is a difference spectrum recorded for the data before and after the electron bombardment; the peaks pointing downward indicate destruction of the precursor (CH_4), and the peaks pointing upward indicate production of products.

crystalline phases of CH_4/N_2 mixtures (Prokhvatilov & Lantsevich 1983; Quirico & Schmitt 1997). Below 20 K, the stable crystalline phase of the CH_4/N_2 mixed solid is the phase (CH_4 II + α N_2); on the other hand, for temperatures between 20 and 35 K, the phase (CH_4 I + α N_2) becomes most stable. Furthermore, nuclear spin conversion of CH_4 occurs rapidly at 20 K, which results in all rotational populations quenching to the $J = 0$ state (Nelander 1985). For a deposition temperature of 33 K, the ν_3 and ν_4 bands took on single, broad, and symmetric features. The crystalline phase of N_2 solid converted to a β-form, and the peak positions shifted to 1300.4 and 3010.6 cm^{-1}. For temperatures over 40 K, the deposition of the N_2 matrix became inefficient; hence, CH_4 was less diluted in solid nitrogen, and the observed bands of CH_4 became broad and unobvious, similarly to the reported spectrum of amorphous-CH_4 at 30 K (Gerakines & Hudson 2015).

3.2. Electron Bombardment of CH_4/N_2 Samples During Deposition

Figure 2 compares the IR spectrum recorded after the electron bombardment of a gaseous CH_4/N_2 sample during deposition with that of a CH_4/N_2 solid. In our previous work (Wu et al. 2013a), the IR spectrum of a CH_4/N_2 matrix sample at 10 K, upon irradiation with 500 eV electrons for 2 hr, produced a large number of hydrocarbons and nitriles, as shown in Figure 2(A); assignments for some prominent peaks are marked for comparison. Because Figure 2(A) is a difference spectrum obtained before and after the electron bombardment of matrix samples, the bands of CH_4 pointed downward for destruction after electron bombardment. Figure 2(B) shows the IR absorption spectrum of a similar matrix sample upon electron bombardment during deposition. CH_3 and N_3 radicals became the most abundant species observed in the matrix. Moreover, nitrile species were seldom formed, as compared to the results of the electron bombardment of solid samples. That is because the observed species in Figure 2(B) are primary products generated from the electron bombardment of gaseous CH_4/N_2 mixtures. Once they condensed onto the cold target to form a solid matrix, they were preserved from further electron bombardment by scattered electrons given the geometry of the electron beam with respect to the cold substrate and that the effective penetration depth of 500 eV electrons is less than 50 nm (Bennett et al. 2013).

In contrast, the electron bombardment of solid samples produced various hydrocarbon and nitriles species, particularly those CN-bearing molecules without H-atoms. During formation, these CN-bearing molecules—such as CN, CN_2, and $(CN)_2$—are required to undergo several dissociation and combination reactions stepwise. Hence, continuous electron bombardment of the same layers of the matrix samples can promote further reactions for producing the secondary or more complex molecules. Table 1 lists the line positions of the observed species upon electron bombardment of the matrix samples during deposition; detailed information of those species observed upon the irradiation of solid samples can be found in our previous work (Wu et al. 2013a).

In separate experiments, electron bombardment of similar matrix samples during deposition at various temperatures was performed in order to understand the effects upon the band structures of products, forming species, and reaction mechanisms. Figures 3(B)–(D) present IR absorption spectra of electron-bombarded matrix samples deposited at 20, 33, and 44 K, respectively; the corresponding spectrum recorded at 10 K is depicted in Figure 3(A) for comparison. By comparing the band positions and band profiles between 10 and 20 K, as shown in Figure 4, one may note that the most obvious change occurs in the ν_3 band of N_3. The doublet features at 1657.8 and 1652.6 cm^{-1} observed at 10 K become a single peak at 20 K, and the line position slightly shifts to 1657.2 cm^{-1}. Similarly, the ν_4 band of CH_3 also changes from the doublet to singlet pattern, though the line position remains at 1406.5 cm^{-1}. The ν_2 band only shows a slight shift from 611.2 cm^{-1} (10 K) to 610.7 cm^{-1} (20 K). Other weak bands observed either with shifts in line positions or changes in band patterns can be found in Table 1. In addition, some bands arose when deposition occurred at 20 K, as indicated by the arrows in Figure 3(B); these bands can be readily assigned to C_2H_6 (816.2, 2891.7, and 2987.0 cm^{-1}), NH_3 (970.0 cm^{-1}), C_2N (1064.4 cm^{-1}), CH_2N_2 (2036.6 cm^{-1}), and $C_3H_2N_2$ (2077.9 cm^{-1}), according to the reported band positions and expected reactions. At a higher temperature, the diffusion of trapped species in the solid matrix is expected to occur more easily. Thus, two CH_3 radicals can combine to form an C_2H_6, which is further supported by the observation of the weaker band of CH_3 in Figure 3(B). NH_3 might be formed from combination reactions of N and H atoms because atomic species have large mobilities in the matrix.

Because the diffusion temperature of solid nitrogen is about 30 K, above this temperature the nitrogen matrix becomes "soft," and the diffusion of trapped species occurs easily. Radicals and unstable molecules can recombine to form more stable molecules. Most IR features of radical species were disappeared, including the bands of CH_3 and N_3, which were observed as the strongest peaks for low-temperature deposition, as shown in Figures 3(C) and (D). Methyl and azide radicals generated in the gas phase might subsequently react with H atoms and N atoms to form CH_4 and N_2, respectively; such radical–radical recombination is barrierless. Because most of the reaction initiators (N_3 and CH_3) were converted back to precursors (CH_4 and N_2) after deposition, it can be imagined that products were seldom observed; only three weak and broad

Table 1
Observed Line Positions (cm^{-1}) of Products upon Irradiation of CH_4/N_2 Matrix Samples at Various Temperatures with 500 eV Electrons[a]

10 K	20 K	30 K	40 K	Assignment	Literature[b]
			502.4	?	
			516.7	?	
			525.9	?	
611.2	610.7			$CH_3(\nu_2)$	$611/N_2$[c]
624.6	624.6			C_4H_2	$627.8/Ne$[d]
	816.2			$C_2H_6(\nu_{12})$	$821/N_2$[e]
862.0 (868.1)	862.0 (868.1)			HCNN (ν_3)	$863/N_2$[f] $871/N_2$[f]
	872.3			H_2CCNH (ν_{11})	$872/Ar$[g]
876.6 (881.9) (882.8)	876.6 (881.6)			$C(NH)_2$ (ν_8)	$886/Ar$[h]
898.5	897.4			C_2H_3	$897.4/Ne$[i]
	970.0			NH_3 (ν_2)	$971/N_2$[e]
1034.5	1034.5			CH_3N (?)	$1029/N_2$[j]
	1064.4			CCN (ν_3)	$1066/Ar$[k]
1406.5 (1391.6)	1406.5			$CH_3(\nu_4)$	$1398/Ar$[l]
1657.8 (1652.6)	1657.2			N_3 (ν_3)	$1657/N_2$[m]
1800.6 (1789.1)	1799.5			HCNN (ν_2)	$1800/N_2$[f]
1874.8	1874.8			HCNC (ν_2)	$1874.2/N_2$[n]
1940.1	1940.1			C_3N^- (ν_2)	$1944.3/Ar$[o]
2003.6 (2005.6)	2003.3			N_3^- (ν_3)	$2002.9/ N_2$[p]
	2036.6			H_2CCNH (ν_3)	$2040/Ar$[g]
		2039.8	2040.4	?	
	2077.9			HNCCHCN	$2070.4/Ar$[q]
		2079.0	2081.2	?	
2096.0 (2100.6)	2096.0 (2100.6)			$C(NH)_2$ (ν_7)	$2097/Ar$[h]
		2105.7	2104.2	?	
2240.4	2235.4			$N_4^+(\nu_3)$	$2237.6/Ne$[r]
	2891.7	2882.9		$C_2H_6(\nu_5)$	$2883/N_2$[e]
	2987.0			$C_2H_6(\nu_{10})$	$2980/N_2$[e]
3166.0 (3158.0)				CH_3 (ν_3)	$3162/Ne$[s]
3287.2	3286.9			HCN (ν_1)	$3286/N_2$[e]
3321.9	3321.9			$C_4H_2(\nu_4)$	$3326.7/Ar$[d]
3566.5				HNC (ν_1)	$3565/N_2$[e]

Notes.
[a] Observed line positions listed in parentheses are the absorptions trapped in minor sites; the "?" mark indicates unknown species or tentative assignments.
[b] The matrix media used for the measurements are listed after the reported numbers.
[c] Milligan & Jacox (1967).
[d] Patten & Andrews (1986).
[e] Moore & Hudson (2003).
[f] Ogilvie (1968).
[g] Jacox (1979).
[h] King & Strope (1971).
[i] Wu et al. (2008).
[j] Ferrante (1987).
[k] Bondybey & English (1978).
[l] Jacox (1977).
[m] Kim & Kaiser (2012).
[n] Maier et al. (1998).
[o] Kolos et al. (2008).
[p] Tian et al. (1988).
[q] Maier & Endres (2000).
[r] Thompson & Jacox (1990).
[s] Snelson (1970).

features appeared in the spectral region of 2000–2200 cm^{-1}. These features, which were observed at 2039.8, 2079.0, and 2105.7 cm^{-1} for 33 K and 2040.4, 2081.2, and 2104.2 cm^{-1} for 44 K, are similar to the observed bands at 10 and 20 K, which can be assigned to CH_2N_2, $C_3H_2N_2$, and $C(NH)_2$, respectively. Hence, these bands might be correlated to those assigned products or other larger nitrile species. Furthermore, this spectral region, which is associated with the strongest absorptions of characteristic CN stretching modes of nitrile species, further supports our tentative assignments.

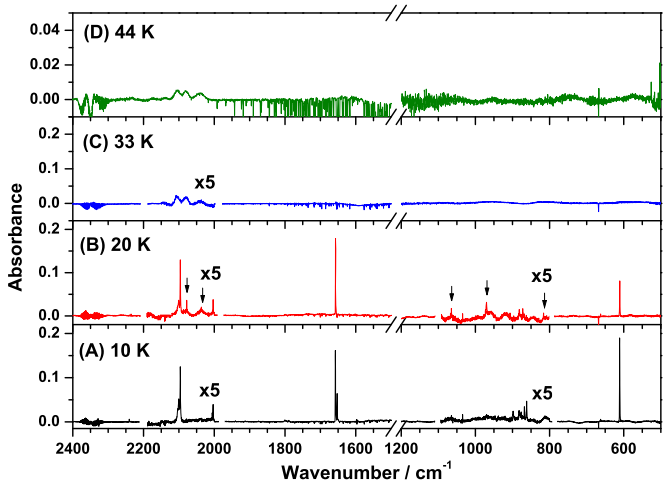

Figure 3. Infrared (IR) absorption spectra of electron-bombarded CH_4/N_2 matrix samples during deposition at (A) 10 K, (B) 20 K, (C) 33 K, and (D) 44 K.

It is worth noting that there are several bands observed near 500–525 cm^{-1}, as shown in Figure 3(D). Above 44 K, nitrogen is less solidified because of large vapor pressures, and fragments generated in the gas phase can undergo further reactions without separation of the N_2 matrix on the cold target. However, these bands are difficult to assign owing to the lack of observation of other spectral features, as well as the typical absorptions of ring-stretching modes of some N-heterocyclic compounds. Furthermore, CC torsional modes of long-chain carbon clusters or nitriles lie in this spectral region, which suggests that the formation of larger and more complex molecules is possible for deposition at higher temperatures.

3.3. UV Absorption Spectra of Electron-bombarded Samples

Figure 5 compares the UV absorption spectra of electron-bombarded matrix samples at various temperatures. The intense and sharp band observed at 272.5 nm, as shown in Figures 5(A)–(C), can be attributed to the electronic transition $A\,^2\Sigma_u^+ \leftarrow X\,^2\Pi_g$ of N_3, which is consistent with our previous works (Wu et al. 2013a). Moreover, the electronic transitions of N_3 from the ground state to states of $2\,^2\Pi_u$, $1\,^2\Sigma_g^+$, and $1\,^2\Sigma_g^-$ also show weak absorptions with fine structures in the 225–198 nm region, which was also reported in our previous work on the electron bombardment of pure solid nitrogen (Wu et al. 2013b). Nevertheless, the progressions of N_3 in the 225–198 nm region are situated on a broad absorption feature that was absent in our previous work (Wu et al. 2013b). By checking the corresponding IR spectra (Figure 3), one can see that CH_3 and N_3 radicals are the most abundant products. Furthermore, the reported absorption of gaseous CH_3 shows the transition from the ground state to the 3 s Rydberg state beginning near 216 nm (Herzberg & Shoosmith 1956). Therefore, we assign this broad feature with maximum absorption at 213.0 nm and a FWHM of 11.6 nm to the electronic transition $B^2A_1' \leftarrow X^2A_2''$ of CH_3 in solid N_2. In addition, for 20 K deposition, another weak progression appears at 311.0, 301.9, 294.2, 286.4, and 279.0 nm with an average interval of 922 cm^{-1}; this progression can be attributed to the electronic transition $A \leftarrow X$ of $H_2C{=}C{=}NH$, which agrees with the band positions recorded at 306.2, 297.0, 288.5, 280.3, and 273.0 nm in solid Ar by Jacox (1979), as compared in Table 2; this is also consistent with our observation of a new IR band of $H_2C{=}C{=}NH$ arising for the case of 20 K deposition.

Compared to results of deposition at lower temperatures, UV absorption features became either weaker or unobservable, as shown in Figure 5(C). Similar behavior was also found in the corresponding IR spectrum, as shown in Figure 3(C). However, UV absorption spectroscopy provides higher sensitivity, and thus a smaller amount of N_3 remains to be detected. At 44 K deposition, almost nothing can be distinguished from the background noise except for a weak, broad band centered at 219.4 nm with a FWHM of 8.9 nm. Based on the corresponding IR spectrum, this broad UV band might be associated with the same carrier that has IR absorptions in the 500–525 cm^{-1} or 2050–2150 cm^{-1} regions, although no studies have reported the electronic transitions of the candidate carriers in this wavelength range. Therefore, we performed quantum chemical calculations to predict the electronic transitions of these candidates, including $C(NH)_2$ and $C_3H_2N_2$, which are tentatively associated with the absorptions in the 2050–2150 cm^{-1} region. The vertical excitation energy of $C_3H_2N_2$ for the $S_2 \leftarrow S_0$ transition predicted at the B3LYP/aug-cc-pVTZ level of theory is about 216 nm. The predicted geometry of $C_3H_2N_2$ in the ground state and the corresponding molecular orbitals for the electronic excitation from S_0 to S_2 are represented in Figures 6 and 7, respectively. This excitation involves the transition of an electron from the π bonding orbital of the C = C bond to the π^* orbital. The predicted excitation energies are close to our observed band centered at 219.4 nm, and arose at 228.6 nm. Therefore, we tentatively assign this broad band to the absorption of $C_3H_2N_2$ or other molecules with similar frameworks.

4. ASTROPHYSICAL IMPLICATIONS

Stern et al. (2012) used the *Hubble Space Telescope* with the Cosmic Origins Spectrograph (*HST*-COS) to record ultraviolet reflectance spectra of Pluto at two rotational phases. An absorption feature between 210 and 240 nm with an absorption maximum near 222 nm was found in the 95° longitude of Pluto. Because most nitriles and/or large hydrocarbons have UV absorptions in this spectral region, they suggested that complex molecules may exist on the surface of Pluto. In our previous works, we recorded the UV absorption spectrum of electron-bombarded CH_4 diluted in solid N_2 at 10 K (Wu et al. 2013a). The observed spectrum revealed a band within the 310–200 nm region, centered at 260 nm and with a shoulder near 220 nm. We further studied the UV spectra of electron-bombarded pure solid N_2 (Wu et al. 2013b), C_2H_2 (Wu et al. 2014), and C_2H_4 (Chen et al. 2015) in solid N_2 at 10 K, but all the recorded spectra showed no significant features near 220 nm. Recent near-IR observations by *New Horizons* reveal that the mixing ratios of CH_4:N_2 ices vary significantly on Pluto's surface. The different temperatures on the surface of Pluto might therefore represent a key factor that affects the ratios.

The temperature on Pluto's surface ranges from 33 to 55 K, which means that laboratory simulations of chemical reactions at 10 K might be improper. As demonstrated by the present work, the products that are form from of matrix samples deposited at various temperatures are clearly different. Radical species, such as CH_3 and N_3, can be preserved completely in solid N_2 at lower temperatures, though they disappear to form more stable species at higher temperatures. This laboratory observation might also suggest that the N_2 ice on Pluto's

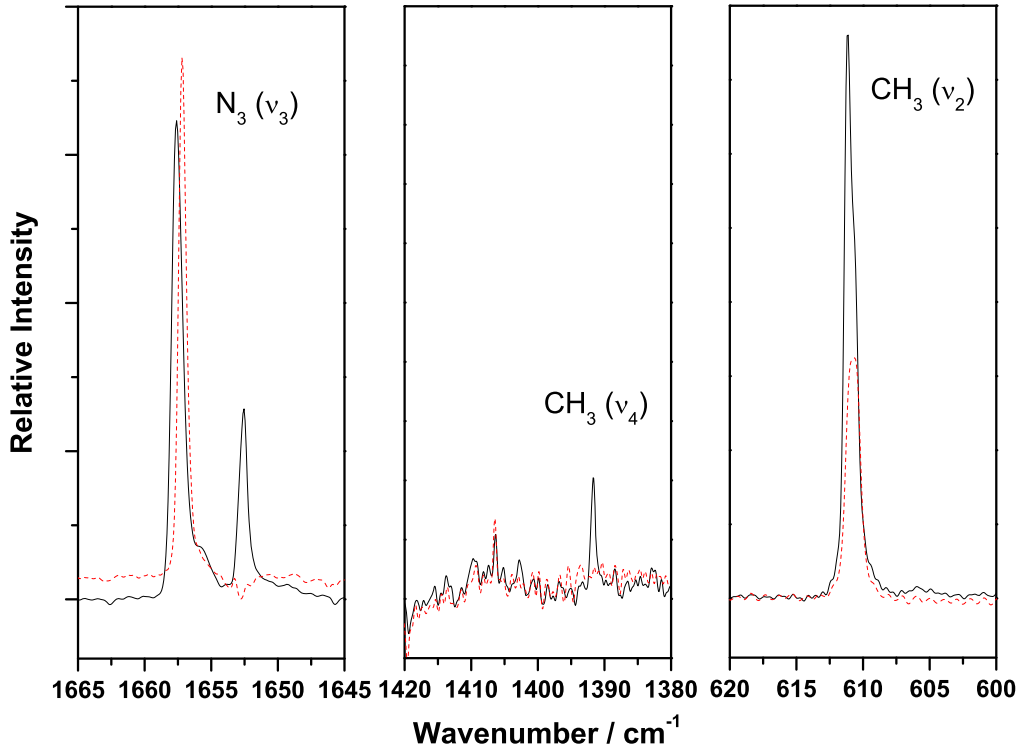

Figure 4. Partial IR spectra of electron-bombarded samples deposited at 10 (solid line) and 20 K (dash line). The assignments for the representing peaks are made.

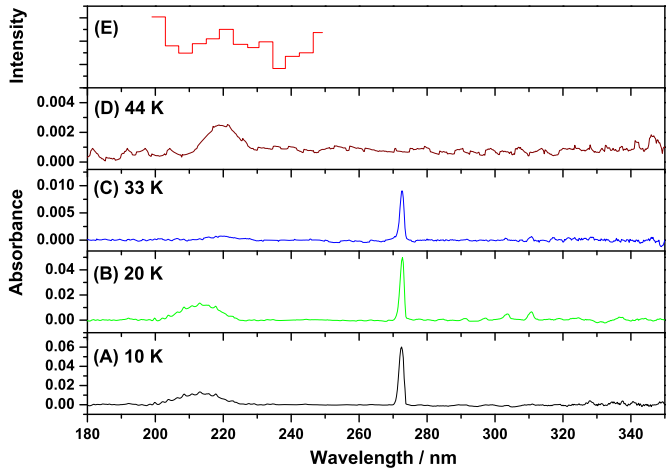

Figure 5. Ultraviolet (UV) absorption spectra of electron-bombarded CH_4/N_2 matrix samples during deposition at (A) 10 K, (B) 20 K, (C) 33 K, and (D) 44 K. (E) The inverted *HST*-COS Pluto spectrum (Stern et al. 2012).

surface is not rigid enough to preserve reactive species, but that reactive species diffuse and combine to form large, complex, and stable species. Therefore, our earlier simulated UV spectra of ices did not reproduce an absorption band similar to that observed on Pluto's surface.

Figure 5(E) depicts a UV reflectance spectrum at the 95° longitude of Pluto recorded by *HST* (Stern et al. 2012); this spectrum is inverted for ease of comparison with laboratory UV absorption spectra. As compared with Figures 5(A)–(C), our results suggest that the absorption of CH_3 and N_3 might have a small contribution to the band shoulder of Pluto's band near 222 nm. Although laboratory results indicate that the amounts of CH_3 and N_3 decrease with increasing temperature, the environment on Pluto exists in a dynamical equilibrium

Table 2
Wavelengths of Band Centers and Band Intervals of $A \leftarrow X$ of H_2CCNH

Literature[a] /nm	λ /nm	Energy[a] /cm^{-1}	Interval /cm^{-1}
306.2	311.0	32154.3	…
297.0	301.9	33123.6	969.2
288.5	294.2	33990.5	866.9
280.3	286.4	34916.2	925.7
273.0	279.0	35842.3	926.1

Note.
[a] Data taken from Jacox (1979) in an Ar matrix.

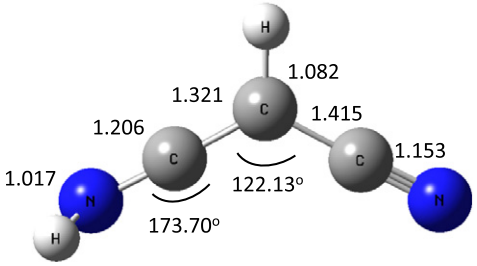

Figure 6. Predicted geometric parameters of $C_3H_2N_2$ in the ground state. The unit of bond length is in Å and the bond angle is in degree.

between its atmosphere and surface. Therefore, the amounts of CH_3 and N_3 may reach a steady state. Compared with Figure 5(D), the *HST* feature is almost identical to our UV absorption spectrum recorded at 44 K in terms of band center, shape, and width. Although the assignment of this absorption remains tentative, the carrier unambiguously belongs to large nitrile species according to our IR diagnostics. Further studies

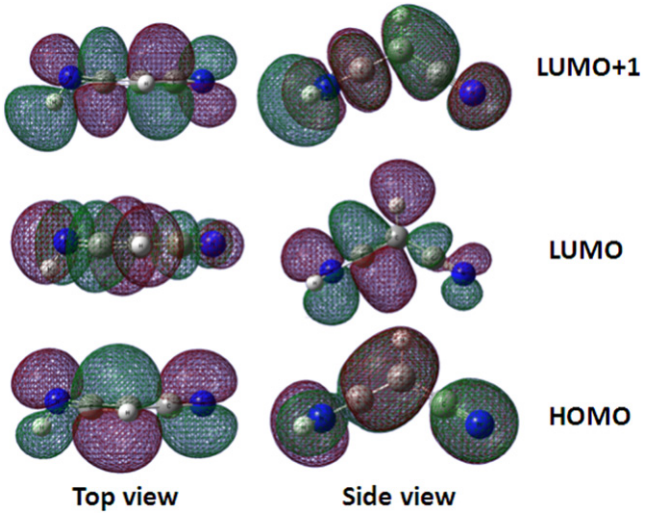

Figure 7. Representative molecular orbitals of $C_3H_2N_2$. For the $S_0 \rightarrow S_2$ transition, electron is excited from HOMO to LUMO+1. HOMO: Highest occupied molecular orbital. LUMO: Lowest unoccupied molecular orbital.

conducted on a temperature-programed desorption technique with mass spectroscopy are in progress for correct assignment of the carriers.

5. CONCLUSIONS

We compared the results of CH_4/N_2 (1/400) matrix samples upon irradiation with 500 eV electrons during matrix deposition and after deposition. According to the observed IR spectra, N_3 and CH_3 radicals were produced predominantly upon electron bombardment during deposition. However, for deposition at higher temperatures, the observed bands of CH_3 and N_3 became either weak or unobservable, and only nitrile species survived. UV absorption spectra of the electron-bombarded ice samples were obtained, and the carriers associated with the absorption bands were assigned according to the observed products identified by IR spectroscopy. In particular, the band centered at 219.4 nm with a FWHM of 8.9 nm (observed for the case of deposition at 44 K) fits well with the absorption features of Pluto's spectrum recorded by *HST*-COS. Our results therefore further confirm that complex nitrile species exist on Pluto's surface.

We thank the Ministry of Science and Technology of Taiwan (MOST 102-2113-M-213-002-MY2) and the NSRRC for financial support.

REFERENCES

Barnett, I. L., Lignell, A., & Gudipati, M. 2012, ApJ, 747, 13
Becke, A. D. 1993, JChPh, 98, 5648
Bennett, C. J., Pirim, C., & Orlando, T. M. 2013, ChRv, 113, 9086
Bohn, R. B., Sandford, S. A., Allamandola, L. J., & Cruikshank, D. P. 1994, Icar, 111, 151
Bondybey, V. E., & English, J. H. 1978, JMoSp, 70, 236
Chen, H.-F., Liu, M.-C., Chen, S.-C., Huang, T.-P., & Wu, Y.-J. 2015, ApJ, 804, 36
Cruikshank, D. P., Grundy, W. M., DeMeo, F. E., et al. 2015, Icar, 246, 82
Cruikshank, D. P., Imanaka, H., & Dalle Ore, C. M. 2005, AdSpR, 36, 178
Cruikshank, D. P., Pilcher, C. B., & Morrison, D. 1976, Sci, 194, 835
Eberhardt, W., Sham, T. K., Carr, R., et al. 1983a, PhRvL, 50, 1038
Eberhardt, W., Stöhr, J., Feldhaus, J., Plummer, E. W., & Sette, F. 1983b, PhRvL, 51, 2370
Ferrante, R. F. 1987, JChPh, 86, 25
Frisch, M. J., Trucks, G. W., Schlegel, H. B., et al. 2009, GAUSSIAN 09, Revision A.02 (Wallingford, CT: Gaussian, Inc.)
Gerakines, P. A., & Hudson, R. L. 2015, ApJL, 805, L20
Gladstone, G. R., Stern, S. A., Ennico, K., et al. 2016, Sci, 351, 1280
Govender, M. G., & Ford, T. A. 2000, JMoSt, 550–551, 445
Grundy, W. M., Binzel, R. P., Buratti, B. J., et al. 2016, Sci, 351, 1283
Grundy, W. M., Olkin, C. B., Young, L. A., Buie, M. W., & Young, E. F. 2013, Icar, 223, 710
Herzberg, G., & Shoosmith, J. 1956, CaJPh, 34, 523
Hodyss, R., Howard, H. R., Johnson, P. V., Goguen, J. D., & Kanik, I. 2011, Icar, 214, 748
Hudson, R. L., & Moore, M. H. 2002, ApJ, 568, 1095
Jacox, M. E. 1977, JMoSp, 66, 272
Jacox, M. E. 1979, CP, 43, 157
Kendall, R. A., Dunning, T. H., Jr., & Harrison, R. J. 1992, JChPh, 96, 6796
Kim, Y. S., & Kaiser, R. I. 2012, ApJ, 758, 37
King, S. T., & Strope, J. H. 1971, JChPh, 54, 1289
Kolos, R., Gronowski, M., & Botschwina, P. 2008, JChPh, 128, 154305
Krasnopolsky, V. A. 2001, Icar, 153, 277
Lee, C., Yang, W., & Parr, R. G. 1988, PhRvB, 37, 785
Lellouch, E., de Bergh, C., Sicardy, B., Kaufl, H. U., & Smette, A. 2011, A&A, 530, L4
Lo, J.-I., Chou, S.-L., Peng, Y.-C., et al. 2015, ApJS, 221, 20
Maier, G., & Endres, J. 2000, Eur. J. Org. Chem., 2000, 2535
Maier, G., Reisenauer, H. P., & Rademacher, K. 1998, CEJ, 4, 1957
Mangina, R. S., Ajello, J. M., West, R. A., & Dziczek, D. 2011, ApJS, 196, 13
Materese, C. K., Cruikshank, D. P., Sanford, S. A., et al. 2014, ApJ, 788, 111
Materese, C. K., Cruikshank, D. P., Sanford, S. A., Imanaka, H., & Nuevo, M. 2015, ApJ, 812, 150
Merlin, F. 2015, A&A, 582, A39
Milligan, D. E., & Jacox, M. E. 1967, JChPh, 47, 278
Moore, M. H., & Hudson, R. L. 2003, Icar, 161, 486
Nelander, B. 1985, JChPh, 82, 5340
Ogilvie, J. F. 1968, CaJCh, 46, 2472
Owen, T. C., Roush, T. L., Cruikshank, D. P., et al. 1993, Sci, 261, 745
Palumbo, M. E., Ferini, G., & Barata, G. A. 2004, AdSpR, 33, 49
Patten, K. O., Jr., & Andrews, L. 1986, JPhCh, 90, 3910
Peterson, K. A., Woon, D. E., & Dunning, T. H., Jr. 1994, JChPh, 100, 7410
Prokhvatilov, A. I., & Lantsevich, L. D. 1983, JLTP, 9, 94
Quirico, E., & Schmitt, E. 1997, Icar, 127, 354
Schindhelm, E., Stern, S. A., Gladstone, R., & Zangari, A. 2015, Icar, 246, 206
Snelson, A. 1970, JPhCh, 74, 537
Song, M.-Y., Yoon, J.-S., Cho, S., et al. 2015, JPCRD, 44, 023101
Stern, S. A. 2010, Natur, 468, 775
Stern, S. A., Bagenal, F., Ennico, K., et al. 2015, Sci, 350, 292
Stern, S. A., Cunningham, N. J., Hain, M. J., Spencer, J. R., & Shinn, A. 2012, AJ, 143, 22
Tegler, S. C., Cornelison, D. M., Grundy, W. M., et al. 2010, ApJ, 725, 1296
Thompson, W. E., & Jacox, M. E. 1990, JChPh, 93, 3856
Tian, R., Facelli, J. C., & Michl, J. 1988, JPhCh, 92, 4073
Wu, Y.-J., Chen, H.-F., Chuang, S.-J., & Huang, T.-P. 2013a, ApJ, 768, 83
Wu, Y.-J., Chen, H.-F., Chuang, S.-J., & Huang, T.-P. 2013b, ApJ, 779, 40
Wu, Y.-J., Chuang, S.-J., Chen, S.-C., & Huang, T.-P. 2014, ApJS, 212, 7
Wu, Y.-J., Lin, M.-Y., Cheng, B.-M., Chen, H.-F., & Lee, Y.-P. 2008, JChPh, 128, 204509
Wu, Y.-J., Wu, C. Y. R., Chou, S.-L., et al. 2012, ApJ, 746, 175